Influence of Interface Gap on Compressive Behaviour of Axially Loaded Square CFST Stub Columns

Manoj Kumar[11](https://orcid.org/0000-0002-4561-794X) and Manigandan R[2]

[1]Department of Civil Engineering, BITS Pilani – Pilani Campus, Pilani (Raj.)–333031, India
manojkr@pilani.bits-pilani.ac.in

[2]Department of Civil Engineering, Saveetha School of Engg., Saveetha Univ., Chennai, India
prof.manigandan.123@gmail.com

Abstract. The axial compressive strength of concrete-filled steel tubular (CFST) columns is significantly improved owing to the lateral confinement offered by the steel tube and the interaction between the steel tube and concrete core. Occasionally, there exists an interface gap between the concrete core and steel tube for several reasons; consequently, the axial load-deformation response of the column is significantly affected. This paper aims to numerically investigate the effect of the interface gap on the axial load-deformation response of axially loaded Square CFST (SCFST) stub columns with different cross-sectional dimensions. To evaluate the effect of interface gap on different-sized SCFST stub columns, the side length of the SCFST section has been varied from 140 mm to 200 mm at an interval of 20 mm, and each column has been analysed for 0 mm, 1 mm and 2 mm interface gap. The non-linear finite element analysis of SCFST columns has been performed using the ABAQUS, where the C3D8R element has been used to discretise the concrete core as well as steel tube, and the Extended Drucker-Prager (E-DP) model has been employed to simulate the plastic behaviour of concrete core. The study shows that the presence of a gap between the concrete core and steel tube marginally reduces the axial compressive strength of the SCFST column; however, it significantly affects the ductility and lateral bulging of the column.

Keywords: Concrete-filled steel tube . Stub column . Interface gap . ABAQUS

1 Introduction

In recent eras, the use of Concrete Filled Steel Tubular (CFST) columns in structural applications has rapidly grown due to their enhanced compressive strength, high ductility, and large energy absorption capacity (Xiao et al., 2005; Kibriya, 2006; Han et al., 2016). The CFST columns exhibit a significant rise in axial compressive strength mainly because of two reasons, firstly, the composite action between the concrete core and steel tube, and secondly, the lateral confining pressure offered by the steel tube to the concrete core. Adequate composite action between the concrete core and steel tube necessitates seamless interaction between the concrete core surface and

inner face of the steel tube, which is usually achieved by an intact bond between these two surfaces, termed a chemical bond (Fujimoto et al., 2004; Wang et al., 2015). Tao et al. (2017) pointed out that the chemical bond strength decreases remarkably with the increase in cross-sectional dimensions. The chemical bond is an elastic brittle shear transfer mechanism that remains active in the early stage of loading until the shear stress at the interface does not exceed the shear resistance offered by the chemical bond action. Once the interface shear stress exceeds the bond shear strength, the chemical bond is broken and this phenomenon is referred to as debonding (Xue et al., 2012; Chen et al., 2019). In the post-debonding phase, shear resistance at the interface is governed by two phenomena: mechanical micro-locking and frictional resistance. The contribution of micro-locking in shear resistance between concrete core and steel tube is found significantly low; therefore, it is usually not accounted for in analysis; however, the frictional resistance between steel tube and concrete core is found substantial and its magnitude depends on the lateral confining pressure exerted by the steel tube and the friction coefficient at the interface of concrete core and steel tube. Though, a substantial amount of uniform lateral confining pressure is experienced by concrete core in circular CFST columns, it becomes highly non-uniform in rectangular/square CFST sections, consequently, only a marginal increase in the axial compressive strength is observed for these sections. Thus the bond strength at the interface of the steel tube and concrete core in the rectangular/square sections becomes important in developing the interface shear resistance.

Nevertheless, in the CFST columns, the bond between the steel tube and the concrete core remains of significant concern owing to improper compaction, shrinkage in concrete, lack of curing of encased concrete, temperature effects, etc., consequently, a gap between the steel tube and concrete core is developed (Shiming and Huifeng, 2012). The occurrence of the gap between the concrete core and steel tube results in failure of the interface bonding action tending no confinement effect, especially in the initial phase of loading (Ho et al., 2014). With the increase in axial load on the CFST column, concrete expands laterally until it comes in contact with the steel tube. Once the gap between the concrete core and steel tube is ceased, the concrete core interacts with the steel tube and experiences lateral confining pressure similar to that in bonded (no gap) CFST columns (Liao et al., 2011).

A significant numbers of experimental and numerical studies have been performed in the past to study the compressive behavior of debonded circular section CFST columns, however, only a few numerical studies appear in the context of debonded non-circular section CFST columns. Qu et al. (2020) experimentally compared the effect of partial (single side) and circumferential (all four sides) gap on the axial compression bearing capacity of rectangular section concrete filled steel tubular (R-CFST) columns. They found that the occurrence of circumferential gap in R-CFST columns greatly reduces the interaction between the steel tube and concrete, consequently, results in a larger axial deformation and a lower bearing capacity of R-CFST columns.

The aim of this paper is to numerically evaluate the impact of interface gap on the axial compressive behavior of S-CFST columns. In this study, the non-linear finite element analysis of S-CFST columns has been carried out using the ABAQUS (2014)

where the plastic behavior of concrete has been simulated using the Extended Drucker-Prager (E-DP) model. For the validation of adopted materials modeling and mesh size, the FE results for C-CFST and S-CFST columns comprising no gap were compared with the experimental data reported in literature by various researchers and numerical results were found to match experimental data reasonably. For investigating the effect of the gap on the axial response of the square section CFST (S-CFST) columns (Fig. 1(a)), a uniform gap 'g' is considered along all the four sides of concrete core, as shown in Fig. 1 (b). For an S-CFST column of side length a and containing gap g on all the four sides of concrete core, gap ratio χ is calculated as $(2g/a)$.

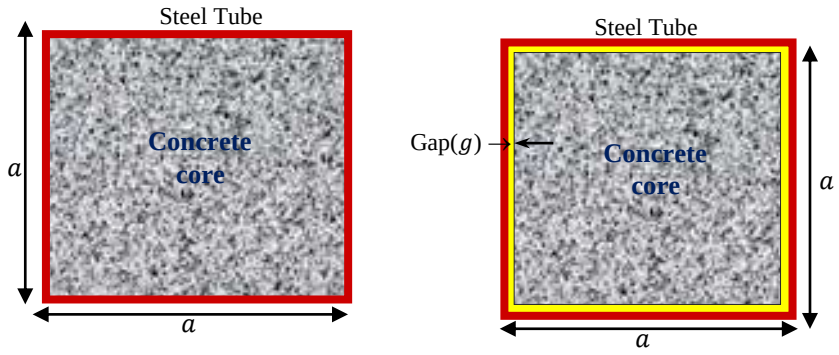

(a) S-CFST Column sectin with no ga (b) S-CFST secion with gap all around

Fig. 1. S-CFST column cross-sections containing (a) no-gap, (b) gap on all four sides

2 Finite Element Modelling of Constituent Materials of CFST

With the use of sophisticated numerical simulations, it is possible to numerically simulate the experimentally observed structural response of CFST columns via non-linear Finite Element (FE) analysis by employing appropriate material modelling techniques for concrete and steel in conjunction with an adequate model for simulating the interaction between the concrete core and steel tube. In the presence of interface gap, concrete core remains unconfined in the initial phase of loading and no confining pressure is experienced by the concrete core. However, with the increase in axial load on the CFST column, the stresses and the equivalent plastic strain in concrete are increased and once the equivalent plastic strain exceeds a certain value, crushing of concrete is initiated. Due to the concrete crushing, concrete core dilates till the initial gap between the concrete core and steel tube is vanished. Owing to subsequent loading on the column, steel tube exerts lateral confining pressure on concrete core and the behaviour of the CFST column with interface gap becomes similar to conventional (no-gap) CFST column. In the FE analysis it becomes tedious to combine two different natures of concrete to simulate the behavior of concrete in the core of CFST column comprising gap. Therefore, the concrete in the core of CFST columns with interface gap is normally modelled as unconfined throughout the loading (Liao et al., 2013) and the same is adopted in present study. In order to numerically predict the compressive

behaviour of S-CFST columns up to the failure stage, it becomes essential to define the stress-strain relation for the unconfined concrete and steel.

2.1 Modelling of Concrete

For simulating the compressive behavior of unconfined concrete, numerous stress-strain models have been developed in past (Popovics, 1973; Carreira and Chu, 1985; Mansur et al., 1995; Attard and Setunge, 1996; Karthik and Mander, 2011; Eltobgy, 2013; Yang et al., 2014). The uniaxial stress-strain model for unconfined concrete proposed by Attard and Setunge (1996) has been found appropriate for modelling the behaviour of concrete core in the debonded S-CFST column (Liao et al., 2013) and the same has been adopted in the present study.

When the current state of stress at a point in material lies within the yield surface, material behaves elastically and once the stress state crosses the yield surface, plastic strains are developed in material and the behavior of material becomes elasto-plastic. To determine whether the material at any state of stress is elastic or has reached the plastic stage, a yield surface needs to be considered. At any stage of loading, the definition of yield surface depends on stress invariants and other variables often called the hardening parameters. Due to the strain hardening, the initial yield surface expands and the final yield surface, where the effective plastic strain equals a certain plastic strain, is referred as failure surface. On the basis of experiments, it is well understood that the yield/failure surface for concrete has curved meridians and its projection on the deviatoric plane is smooth, convex, and exhibits three-fold symmetry (Chen, 1982). To fulfill these requirements several yield criteria have been proposed by numerous researchers (Chen, 1982). Among these failure criteria, the Drucker-Prager (DP) yield criterion is found to be adequate for modeling the hydrostatic pressure dependent materials such as concrete. The DP yield surface is the modified form of the Mohr-Coulomb yield surface whose projection on the deviatoric plane, referred as yield locus, is irregular and contains corners. In order to circumvent the singularities associated with the corners in the yield locus of the Mohr-Coulomb yield surface, the yield locus of the DP model in the deviatoric plane is obtained by circumscribing the exterior angular points of Mohr-Coulomb yield criterion. Since, in the DP model the projection of yield surface on the deviatoric plane is circular in shape, which makes the DP model inadequate to precisely simulate the behaviour of materials having the tensile strength considerably lower than its compressive strength such as concrete. In order to incorporate the effect of different strengths of material in compression and tension, the DP model was modified known as Extended Drucker-Prager (E-DP) yield criterion (Lu et al., 2007; Yu et al., 2010). The E-DP yield criterion is available in ABAQUS (2014) in three different forms namely Linear, Hyperbolic and Exponential. In the present study, the linear E-DP yield criterion with isotropic hardening has been adopted to simulate the behaviour of concrete in the core of CFST column.

2.2 Modelling of Steel

In order to capture the non-linear behavior of steel in the tube, a five-stage stress-strain model has been adopted in present study. The five-stage stress-strain model includes an elastic region $(O-A)$, elasto-plastic region $(A-B)$, plastic region $(B-C)$, strain hardening region $(C-D)$, and the secondary plastic region $(D-E)$ as shown in Fig. 2 (Han et al., 2007). For a steel having yield strength f_{sy}, the stress-strain relation is assumed linear up to the proportional limit, $f_{sp}(=0.8f_{sy})$ and its behavior is considered perfectly plastic when the stress in steel attains the ultimate stress, $f_{su}\ (=1.6f_{sy})$. The stress-strain relations for steel in different regions are defined in Eq. (1).

$$\begin{array}{lll} \text{Elastic region } (O-A) & f=E_s\varepsilon & \varepsilon \le \varepsilon_1\ (=0.8f_{sy}/E_s) \\ \text{Elasto-plastic region } (A-B) & f=-a\varepsilon^2+b\varepsilon+c & \varepsilon_1<\varepsilon\le\varepsilon_2\ (=1.5\ \varepsilon_1) \\ \text{Plastic region } (B-C) & f=f_{sy} & \varepsilon_2<\varepsilon\le\varepsilon_3(=10\varepsilon_2) \\ \text{Strain-hard. region } (C-D) & f=f_{sy}\left[1+0.6\dfrac{\varepsilon-\varepsilon_3}{\varepsilon_4-\varepsilon_3}\right] & \varepsilon_3<\varepsilon\le\varepsilon_4(=100\varepsilon_2) \\ \text{Sec. plastic region } (D-E) & f=1.6f_{sy} & \varepsilon>\varepsilon_4 \end{array} \quad (1)$$

where, E_s is the modulus of elasticity of steel and parameters a, b and b used for defining the stress in elastic-plastic region are defined in Eq. (2).

$$a=\frac{0.2f_{sy}}{(\varepsilon_2-\varepsilon_1)^2};\qquad b=2A\varepsilon_2;\qquad c=0.8f_{sy}+A\varepsilon_1^2-B\varepsilon_1 \quad (2)$$

where, $\varepsilon_1, \varepsilon_2, \varepsilon_3$, and ε_4 are the strains corresponding to stresses at $A, B, C, and\ D$, respectively.

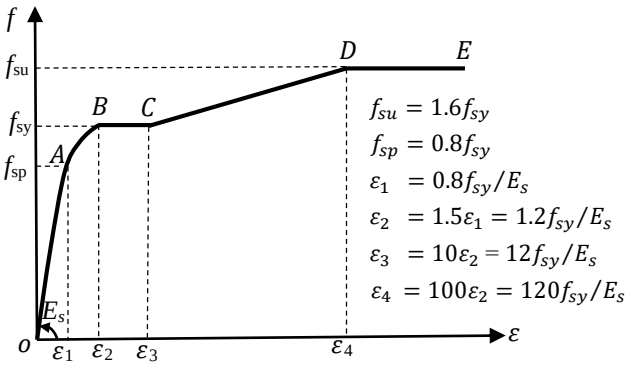

Fig. 2. Stress-strain Model for steel

2.3 Geometrical Details and Material Properties of S-CFST Sections

To examine the influence of interface gap on the axial compressive strength, ductility, and lateral bulging of S-CFST short columns, a parametric study was

conducted. The steel tube thickness and column length were kept constant to 3.8 mm and 540 mm respectively, while the square section's side length was varied from 140 mm to 200 mm, with 20 mm increments. For each of the four sections considered, gaps of 1 mm and 2 mm were introduced between the square-section concrete core and the steel tube on all four sides of the column cross-section. The sections with no gap between concrete core and steel tube were considered as control sections. For all the CFST cross-sections analysed in this study, the modulus of elasticity, yield strength and Poisson's ratio of steel were taken as 200 GPa, 360 MPa and 0.3, respectively. For the infill concrete, the cube compressive strength and Poisson's ratio are taken as 51.28 MPa and 0.2, respectively and the modulus of elasticity of concrete is calculated $4730\sqrt{f_c'}$ where $f_c'$is the cylindrical compressive strength of concrete.

2.4 Finite Element Meshing and Boundary Conditions

For the finite element analysis of CFST columns using the FE software ABAQUS, the eight-node reduced integration based solid brick linear element C3D8R is usually used to discretize both concrete core and steel tube (Hu et al., 2003; Sakino et al., 2004; Kuranovas et al., 2009; Chung, et al., 2013; Romero et al. 2017; Chen et al., 2019; Seok et al., 2020) and the same has been used in this study to discretize the C-CFST and S-CFST columns. In order to coincide the nodes of concrete core and steel tube in the S-CFST column, the number of elements for discretizing the concrete core along the length and side length of section were kept similar to those corresponds to the steel tube. The mesh sensitivity analysis revealed that discretizing the S-CFST column length in to twenty elements and discretizing the side length of section into seven elements produced the FE results closer to experimental data. A typical finite element discretization of S-CFST column is shown in Fig. 3 where the C3D8R element is discretize concrete core as well as steel tube.

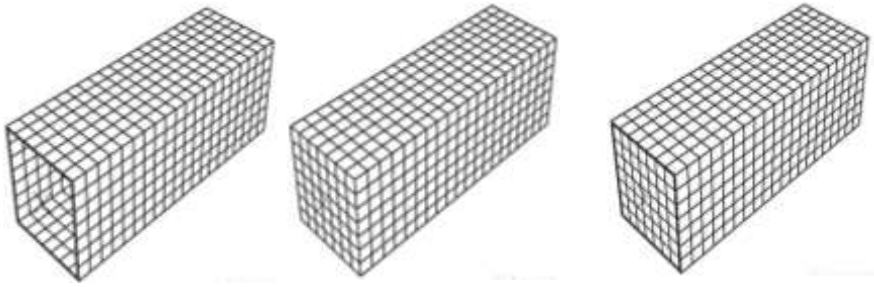

(a) Steel tube (b) Concrete core (c) Steel Tube with concrete core

Fig. 3. Finite Element Discretization for a typical S-CFST column

For the application of boundary conditions and axial load on S-CFST columns in the FE software ABAQUS, the reference points RP1 and RP2 were considered at the top and bottom faces of the column, respectively as shown in Fig.4. All the nodes of the concrete core and steel tube located at the top face of the column were connected to RP1 via rigid ties, and in the similar way, all the nodes of the concrete core and steel tube located at the bottom face were connected to RP2. While determining the axial

compressive strength of column via experiments, normally rigid steel plates are attached to top and bottom faces of column and these plates restrain the rotations at the ends of the column. In order to replicate the boundary conditions experienced by the S-CFST column during the tests performed in laboratory, the bottom reference point RP2 was fully restrained $(i.e. u_x = u_y = u_z = \theta_x = \theta_y = \theta_z = 0)$ while the reference point RP1 was allowed to displace along the axis of column only $(i.e.\ u_x = u_y = \theta_x = \theta_y = \theta_z = 0;\ u_z \neq 0)$ as shown in Fig. 4. In this study the displacement control approach was adopted, therefore, the concentric axial load was applied at RP1 in the form of displacement.

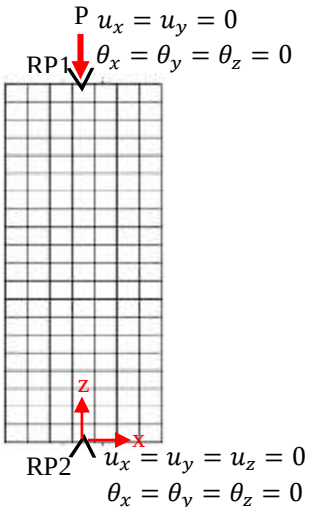

Fig. 4. Location of Reference points and Boundary conditions

3 Influence of Interface Gap on Behaviour of S-CFST Columns

The effect of the interface gap on the axial response of the column was examined on the ultimate compressive strength, axial load-strain variation, and lateral bulging of the S-CFST columns. For comparing the effect of gap on the S-CFST columns with different side-lengths, the compressive strength as well as well as the magnitude of gap are expressed in normalized form. The axial compressive strength of columns with 1 mm and 2 mm gap, $P_{u,1}$ and $P_{u,2}$, respectively, are normalized by the axial compressive strengths of identical section columns with no-gap (control section), $P_{u,0}$. For normalizing the magnitude of gap between concrete core and steel tube (g), the total gap on opposite faces of section $(2g)$ is divided by the side length (a) of column, denoted as gap ratio $\chi\ (= 2g/a)$. For all the S-CFST sections, the normalized strengths $(P_{u,1}/P_{u,0})$ and $(P_{u,2}/P_{u,0})$, and the gap ratios χ_1 and χ_2 for 1 mm and 2 mm interface gap, respectively are summarized in Table 1.

3.1 Impact of Interface Gap on Ultimate Compressive Strength

It can be observed from Table 1 that for both 1 mm and 2 mm interface gaps, the smaller section (140 mm) columns produce lowest strength ratios $(P_{u,1}/P_{u,0})$ and $(P_{u,2}/P_{u,0})$, respectively and these strength ratios improve with the increase in section dimensions. For an interface gap (g), the strength gain with the increase in square section side length (a) may be attributed due to drop in gap ratio $\chi\ (=2g/a)$ which reduces from 1.42 to 1.0 for 1 mm gap and from 2.84 to 2.0 for 2 mm gap. Furthermore, it may be noted that even for the smallest section (140 mm) the drops in ultimate strength for 1 mm and 2 mm gaps are only 1.9% and 3%, respectively. This is because once the concrete dilates, the debonded S-CFST section behaves analogously to corresponding bonded section.

Table 1. Impact of Interface Gap on Axial Compressive Response of S-CFST Columns

Side length, a (mm)	Tube thickness, t (mm)	Tube Slenderness ratio, (a/t)	g = 0 mm			g = 1 mm					g = 2 mm				
			Ult. Strength, $P_{u,0}$ (kN)	Max. Lat. Disp. $\delta_{u,0}$ (mm)	$(\delta_{u,0}\backslash P_{u,0})(mm/mN)$	Gap ratio, χ_1 (%)	Ult. Strength $P_{u,1}$ (kN)	Strength ratio $(P_{u,1}\backslash P_{u,0})$	Max. Lat. Disp., $\delta_{u,1}$ (mm)	$(\delta_{u,1}\backslash P_{u,1})(mm/mN)$	Gap ratio, χ_2 (%)	Ult. Strength $P_{u,2}$ (kN)	Strength ratio $(P_{u,2}\backslash P_{u,0})$	Max. Lat. Disp., $\delta_{u,2}$ (mm)	$(\delta_{u,2}\backslash P_{u,2})(mm/mN)$
140	3.8	36.8	1687	37.9	22.5	1.42	1655	0.981	21.7	13.1	2.84	1636	0.970	19.4	11.9
160	3.8	42.1	2098	17.3	8.3	1.24	2070	0.987	16.9	8.2	2.52	2038	0.971	17.1	8.4
180	3.8	47.4	2560	14.4	5.6	1.12	2527	0.987	16.9	6.7	2.24	2501	0.977	14.4	5.8
200	3.8	52.6	3024	19.3	6.4	1.00	3012	0.996	18.5	6.2	2.00	2980	0.985	16.9	5.7

3.2 Impact of Interface Gap on Axial Load- Strain Response

Fig. 5 illustrates a comparison of axial load-strain curves for S-CFST columns with different tube slenderness ratios (a/t) for the three gaps: 0 mm, 1 mm and 2 mm resulting in gap ratios: 0, 1.43, and 2.86, respectively. Nevertheless, there was minor impact of interface gap on the ultimate compressive strength of columns (as discussed above), the post-peak response of columns is significantly affected by a presence of a gap as shown in Fig. 5. It may also be observed from the figure that the S-CFST columns having slenderness ratio $(a/t)\ up\ to \approx 47$ are unable to exhibit ductility for both 1 mm gap (χ =1.43%) and 2 mm gap (χ = 2.86%) cases. Furthermore, the figure illustrates that sections with larger slenderness ratios $(a\ /\ t\ \geq\ 53)$ tend to exhibit no ductility for a 2 mm gap $(\chi =\ 2.86\%)$; however, in the case of a 1 mm gap $(\chi =\ 1.0\%)$, they display sufficient ductility before failure similar to those with without a gap. This observation suggests that sections with larger slenderness ratios $(a\ /\ t\ \geq\ 53)$ may demonstrate adequate ductility, provided the gap ratio is limited to 1.0%.

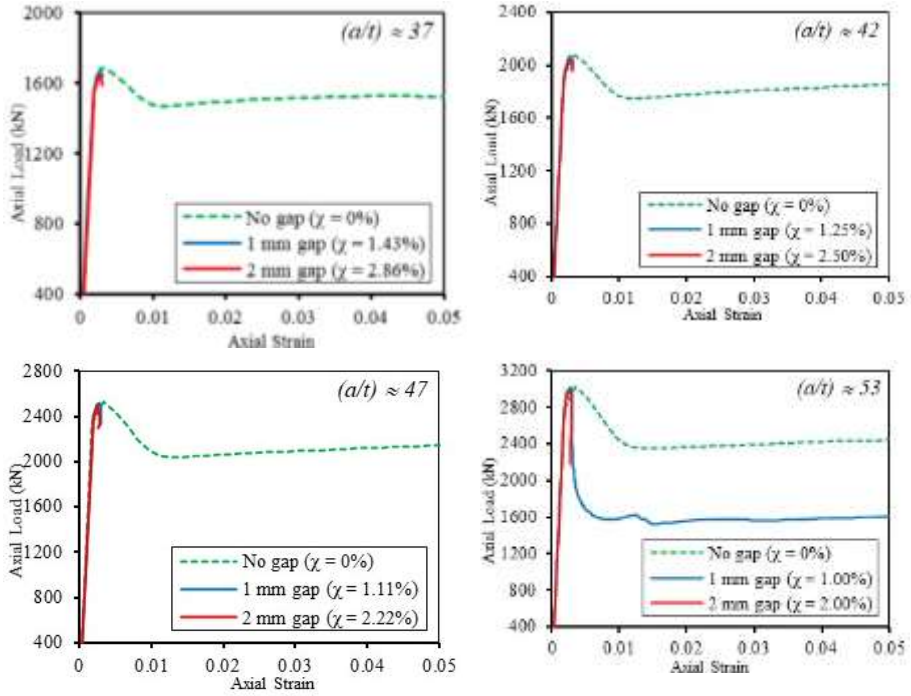

Fig. 5. Effect of Interface gap and tube slenderness ratio on the Axial Load-Strain response of S-CFST columns

3.3 Effect of Interface Gap on Lateral Bulging of S-CFST Columns

With the increase in axial load on debonded S-CFST columns, the equivalent plastic strain in concrete increases and once the equivalent plastic strain exceeds concrete crushing strain, concrete dilates and after vanishing the interface gap, the concrete pushes steel tube, consequently a lateral confining pressure is excreted by steel tube on the concrete core and the column bulges out. Fig. 6 compares the numerically obtained failure modes of a typical S-CFST column (140 mm side length) with interface gaps of 0 mm (no gap), 1 mm, and 2 mm to illustrate the effect of the interface gap on bulging at the ultimate stage. From the figure it may be visualized that irrespective to magnitude of interface gap the maximum lateral displacement, termed as bulging, occurs in the vicinity of mid-height of column.

Table 1 presents the numerically predicted maximum lateral displacements in various S-CFST columns comprising 0, 1 mm, and 2 mm gaps, denoted as $\delta_{u,0}$, $\delta_{u,1}$, and $\delta_{u,2}$ respectively. To evaluate the extent of bulging in S-CFST columns of different cross-sectional dimensions, the bulging phenomenon was quantified in terms of the maximum lateral displacement per unit load. For various cross-sections considered, the magnitudes of $(\delta_{u,0} \,/\, P_{u,0})$, $(\delta_{u,1} \,/\, P_{u,1})$, and $(\delta_{u,2} \,/\, P_{u,2})$ for interface gaps of 0, 1 mm, and 2 mm, respectively are evaluated in Table 1.

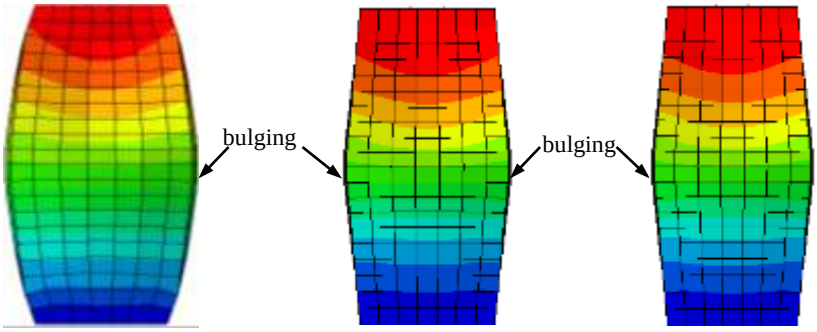

Fig. 6. Effect of Gap on bulging in a typical S-CFST Column (a =140 mm)

Moreover, to examine the effect of tube slenderness ratio (a/t) on bulging in columns comprising with different interface gaps, the variations in $(\delta_{u,0}/P_{u,0})$, $(\delta_{u,1}/P_{u,1})$ and $(\delta_{u,2}/P_{u,2})$ with (a/t) for 0, 1 and 2 mm interface gaps were examined. It may be observed from the Table 1 that as the section side length increases from 140 mm to 200 mm (or the tube slenderness ratio increases from 36.8 to 52.6), the bulging in column with no interface gap decreases from 22.5 mm/mN to 6.4 mm/mN, whereas for the 1 mm gap the bulging reduces from 21.7 to 18.5 and the same reduces from 11.9 to 5.7 mm/mN for 2 mm gap. Also, for both 1 mm and 2 mm gaps, the bulging in the S-CFST columns decreases with a reduction in gap ratio χ. Furthermore, the table shows that the smallest section $(a/t = 36.8)$ with 1 mm gap exhibits the bulging almost two times of that with 2 mm gap, however, for other section dimensions the bulging for 1 mm and 2 mm gaps are comparable. Also, the table suggests smaller debonded S-CFST $(a/t = 36.8)$ sections exhibit lower bulging compared to bonded one.

4 Conclusions

The objective of this study was to conduct numerical investigations on the impact of the interface gap between the steel tube and concrete on the compressive behaviour of square-section concrete-filled steel tubular (S-CFST) columns. For this purpose, while maintaining a constant steel tube thickness (t = 3.8 mm) and column length (L = 540 mm), the side length of the square section (a) was varied from 140 to 200 mm at 20 mm intervals. Each section was subsequently analyzed with 0, 1, and 2 mm interface gaps (g) on all the four side faces of the square-section column. The following conclusions were drawn from this investigation:

- The axial compressive strength of the S-CFST columns in the presence of an interface gap was found consistently lower than that of the analogous bonded $(g = 0)$ columns. For the smaller section (140 mm) the reduction in ultimate strength was 1.9% and 3% for 1 mm and 2 mm gaps, respectively, while the strength reductions dropped to 0.4% and 3.2% for the larger section (200 mm).
- Although the presence of an interface gap resulted in a marginal fall in the compression strength of S-CFST columns, it led to a significant reduction in the

ductility of columns with a side-length (a) to tube-thickness (t) ratio up to approximately 47. Furthermore, the larger section column ((a)/t=53) with a smaller gap (1% of side length) did not exhibit a notable decrease in ductility compared to analogous bonded sections.

- For both 1 mm and 2 mm gaps, the bulging in the S-CFST columns was observed to decrease with a reduction in gap ratio χ. Moreover, the smallest section (140 mm) with 1 mm gap exhibited the bulging almost two times of that with 2 mm gap, however, for other section dimensions the bulging for 1 mm and 2 mm gaps were comparable. Also, smaller debonded S-CFST ($a/t = 36.8$) sections was found exhibit lower bulging compared to bonded one.

References

1. ABAQUS (2014) Analysis user's manual 6.14-EF, Dassault Systems Simulia Corp., Providence.
2. Attard MM and Setunge S (1996) Stress-strain relationship of confined and unconfined concrete. *ACI Materials Journal*.93(5): 432-442. DOI:10.14359/9847
3. Carreira DJ and Chu KD (1985) Stress-Strain Relationship for Plain Concrete in Compression. *ACI Structural Journal* 82(6): 797-804.
4. Chen WF *Plasticity in Reinforced Concrete* (1982), New York: McGraw-Hill.
5. Chen H, Xu B, Zhou T and Mo YL (2019) Debonding detection for rectangular CFST using surface wave measurement: Test and multi-physical fields numerical simulation *Mechanical Systems and Signal Processing* 117:238-254. DOI:10.1016/j.ymssp.2018.07.047
6. Chung KS, Kim JH and Yoo JH (2013) Experimental and analytical investigation of high-strength concrete-filled steel tube square columns subjected to flexural loading *Steel and Composite Structures.* 14(2):133-153. DOI:10.12989/scs.2013.14.2.133
7. Eltobgy HH (2013) Structural design of steel fibre reinforced concrete in-filled steel circular columns. *Steel and Composite Structures*14(3):267-282. doi:10.12989/scs.2013.14.3.267
8. Fujimoto T, Mukai A, Nishiyama I and Sakino K (2004) Behavior of Eccentrically Loaded Concrete-Filled Steel Tubular Columns. *Journal of Structural Engineering* 130(2):203-212. DOI:10.1061/(ASCE)0733-9445(2004)130:2(203)
9. Han LH, Ye Y and Liao FY (2016) Effects of Core Concrete Initial Imperfection on Performance of Eccentrically Loaded CFST Columns. *Journal of Structural Engineering* 142(12):1-13. DOI:10.1061/(asce)ST.1943-541X.0001604
10. Ho JCM, Lai MH and Luo L (2014) Uniaxial behaviour of confined high-strength concrete-filled-steel-tube columns. *Proceedings of the Institution of Civil Engineers: Structures and Buildings* 167(9):520-533. DOI:10.1680/stbu.13.00004
11. Hu H-T, Huang C-S, Wu M-H and Wu Y-M (2003) Nonlinear Analysis of Axially Loaded Concrete-Filled Tube Columns with Confinement Effect. *Journal of Structural Engineering* 129(10):1322-1329. DOI:10.1061/(asce)0733-9445(2003)129:10(1322)
12. Karthik MM and Mander JB (2011) Stress-Block Parameters for Unconfined and Confined Concrete Based on a Unified Stress-Strain Model. *Journal of Structural Engineering* 137(2):270-273. DOI:10.1061/(asce)st.1943-541x.0000294
13. Kibriya T (2006) Performance of short CFST columns using SCC with blended cement. *Proceedings of the Structures Congress and Exposition* 2006:76. DOI:10.1061/40889(201)76
14. Kuranovas A, Goode D, Kvedaras AK and Zhong S (2009) Load-bearing capacity of concrete-filled steel columns. *Journal of Civil Engineering and Management*. 15(1):21-33. DOI:10.3846/1392-3730.2009.15.21-33
15. Liao FY, Han LH and He SH (2011) Behavior of CFST short column and beam with initial

concrete imperfection: Experiments. *Journal of Constructional Steel Research*. 67(12):1922-1935. DOI:10.1016/j.jcsr.2011.06.009

16. Liao FY, Han LH and Tao Z (2013) Behaviour of CFST stub columns with initial concrete imperfection: Analysis and calculations. Thin-Walled Structures 70:57-69. DOI:10.1016/j.tws.2013.04.012
17. Lu FW, Li SP and Sun G (2007) Nonlinear equivalent simulation of mechanical properties of expansive concrete-filled steel tube columns. *Advances in Structural Engineering*. 10(3):273-281. doi:10.1260/136943307781422271
18. Mansur MA, Wee TH and Chin MS (1995) Derivation of the complete stress-strain curves for concrete in compression. *Magazine of Concrete Research* 47(173):285-290. DOI:10.1680/macr.1995.47.173.285
19. Qu X, Huang F, Sun G, Liu Q and Wang H (2020), Axial compressive behaviour of concrete-filled steel tubular columns with interfacial damage, Advances in Structural Engineering, 23(6):1–14, DOI: 10.1177/1369433219891639.
20. Popovics S (1973) A numerical approach to the complete stress-strain curve of concrete. *Cement and Concrete Research*. 3(5):583-599. DOI:10.1016/0008-8846(73)90096-3
21. Richart FE, Brandtzaeg A and Brown RL (1928) A study of the failure of concrete under combined compressive stresses. *Bulletin No 185 Engineering Experiment Station*. 26(12):7-92. http://hdl.handle.net/2142/4277
22. Romero ML, Ibañez C, Espinos A, Portolés JM and Hospitaler A (2017) Influence of Ultra-high Strength Concrete on Circular Concrete-filled Dual Steel Columns. *Structures* 9:13-20. DOI:10.1016/j.istruc.2016.07.001
23. Sakino K, Nakahara H, Morino S and Nishiyama I (2004) Behavior of centrally loaded concrete-filled steel-tube short columns *Journal of Structural Engineering* 130(2):180-188. DOI:10.1061/(ASCE)0733-9445(2004)130:2(180)
24. Seok S, Haikal G, Ramirez JA, Lowes LN and Lim J (2020) Finite element simulation of bond-zone behavior of pullout test of reinforcement embedded in concrete using concrete damage-plasticity model 2 (CDPM2). *Engineering Structures* 221(5):110984. DOI:10.1016/j.engstruct.2020.110984
25. Shiming C and Huifeng Z (2012) Numerical analysis of the axially loaded concrete filled steel tube columns with debonding separation at the steel-concrete interface *Steel and Composite Structures* 13(3):277-293. DOI:10.12989/scs.2012.13.3.277
26. Tao Z, Song TY, Uy B and Han LH (2017) Bond behavior in concrete-filled steel tubes. *Journal of Constructional Steel Research* 120 (6):81-93. doi:10.1016/j.jcsr.2015.12.030
27. Wang R, Han LH, Zhao XL and Rasmussen KJR (2015) Experimental behavior of concrete filled double steel tubular (CFDST) members under low velocity drop weight impact *Thin-Walled Structures* 97:279-295. DOI:10.1016/j.tws.2015.09.009
28. Xiao Y, He W and Choi K (2005) Confined Concrete-Filled Tubular Columns *Journal of Structural Engineering* 131(3):488-497. DOI:10.1061/(ASCE)0733-9445(2005)131:3(488)
29. Xue JQ, Briseghella B and Chen BC (2012) Effects of debonding on circular CFST stub columns *Journal of Constructional Steel Research* 69(1):64-76. DOI:10.1016/j.jcsr.2011.08.002
30. Yang Y, Wang Y and Fu F (2014) Effect of reinforcement stiffeners on square concrete-filled steel tubular columns subjected to axial compressive load *Thin-Walled Structures* 82:132-144. DOI:10.1016/j.tws.2014.04.009
31. Yu M, Zha X, Ye J and She C (2010) A unified formulation for hollow and solid concrete-filled steel tube columns under axial compression *Engineering Structures* 32(4):1046-1053. DOI:10.1016/j.engstruct.2009.12.031